Metastability and Instability in the Lennard-Jones Fluid Investigated by Transition-Matrix Monte Carlo[†,‡]

Vincent K. Shen*

Physical and Chemical Properties Division, National Institute of Standards and Technology, 100 Bureau Drive MS 8380, Gaithersburg, Maryland 20899-8380

Jeffrey R. Errington*

Department of Chemical and Biological Engineering, University at Buffalo, The State University of New York, Buffalo, New York 14260

Received: March 15, 2004; In Final Form: June 25, 2004

Grand canonical transition-matrix Monte Carlo is used to investigate kinetic and thermodynamic stability limits of the liquid and vapor in the Lennard-Jones fluid. Kinetic spinodals are associated with a vanishing of the free-energy barrier between metastable and stable states, and thermodynamic spinodals are related to diverging thermodynamic response functions. We show that the kinetically and thermodynamically defined spinodals are conceptually equivalent viewpoints in the case of the liquid−vapor transition. In agreement with the work of others, we find that the properties of the supersaturated vapor at its limit of stability approach their saturation values with increasing system size. We also find an analogous trend in the case of the superheated liquid. Finally, the computational algorithm and manipulation of data outlined in this work provide an intuitive and efficient method for determining thermophysical properties of stable and metastable fluids via molecular simulation.

I. Introduction

A fluid existing outside its normal range of thermodynamic stability is said to be metastable. As curious as this apparent violation of thermodynamics might seem, metastable fluids occur quite naturally and play crucial roles in our physical world.[1] For example, rain drops form within supersaturated vapors in the upper atmosphere.[2] The transport of nutrients in plants and trees occurs by the ascension of sap under tension from their roots up to their leaves.[3,4] In industrial settings, superheated liquids often play unwanted roles because of their propensity to transform into the vapor phase, cavitation erosion, explosive boiling, and hazardous vapor explosions being well-known examples of the impressive physical damage superheated liquids can inflict.[5−8] Finally, from a technological perspective, supercooled liquids provide the medium in which the important processes of vitrification and crystallization take place.[1,9,10] Despite the prominent roles that metastable fluids play in nature, industry, and technology, they represent a fundamental gap in our understanding of matter at the microscopic level. Here, we focus on pure supersaturated vapors and superheated liquids. For clarity, the former is simply defined to be a vapor that is metastable with respect to the liquid phase, and the latter is a liquid that is metastable with respect to the vapor phase.

From a theoretical perspective, the study of metastable fluids remains a formidable scientific challenge. The reason for this is that the rigorous study of metastability requires the imposition of constraints that prevent the system from relaxing toward stable equilibrium. Although formulating these constraints within a statistical mechanical framework has proven to be a challenging task,[1] classical thermodynamics provides well-defined stability criteria for characterizing the relative stability of a substance. For example, in pure fluids, the focus of this paper, the thermodynamic response functions, such as the isothermal compressibility or isobaric heat capacity, all diverge simultaneously at a limit of stability.[1,11] The locus of state points for which this is true is called the thermodynamic spinodal and represents an absolute stability limit. In this work, we refer to this as a thermodynamic limit of stability because of its origin in thermodynamic stability arguments. Knowledge of such limits is crucial in studying the kinetics of phase transitions, in particular, nucleation where the starting condition must be by definition metastable. From a practical point of view, knowledge of the range of metastability is important in the processing of materials, where a particular morphology is desired.

Conceptually, metastable states represent relative local minima on a system's free-energy surface. However, given enough time, a system originally located in a local minimum will eventually find its way to the global one. The process by which this occurs is called nucleation and growth and entails the initial formation of nuclei of the incipient phase followed by their subsequent growth into macroscopic size. Because the free-energy surface, that is to say, the relationship between the system's free energy and its degrees of freedom, is a highly multidimensional object, it is convenient to project the system's many degrees of freedom onto a single order parameter or reaction coordinate. This simplified perspective of the free-energy surface provides a picture of the transition from metastability to eventual equilibrium in terms of the canonical chemical reaction A → B, where species A represents the metastable system and species B corresponds to the system at stable equilibrium. Thus, by

[†] Part of the special issue "Frank H. Stillinger Festschrift".

[‡] Contribution of the National Institute of Standards and Technology, not subject to U.S. copyright.

* E-mail: vincent.shen@nist.gov; jerring@buffalo.edu.

10.1021/jp040218y CCC: $27.50
Published on Web 09/11/2004

analogy, the rate of the overall phase transition can be described qualitatively by an Arrhenius rate law for activated kinetics. In particular, the rate of nucleation, that is, the rate of formation of nuclei of the stable phase per unit volume, is generally expressed as

$$J = k \exp(-\beta W_b) \tag{1}$$

where k is a kinetic frequency factor that is relatively insensitive to temperature, β is the Boltzmann factor ($\beta = 1/k_B T$ where k_B is the Boltzmann constant and T is temperature), and W_b is the free-energy barrier that the metastable system must traverse. Because of the exponential dependence of the nucleation rate on the barrier height, most studies of nucleation focus on the calculation of this quantity. From a classical point of view,[1] in pure fluids, the barrier height for the liquid−vapor (liquid-to-vapor and vapor-to-liquid) transition is infinitely high at saturation and then decreases monotonically as the system moves away from phase coexistence or becomes increasingly metastable. In fact, the barrier separating the metastable fluid from the stable one eventually vanishes at some degree of penetration into the liquid−vapor phase coexistence dome. Under these conditions, the system is said to be unstable because it is no longer required to traverse an energy barrier but instead can evolve *spontaneously* to the equilibrium state. Although the free-energy barrier, W_b, is a thermodynamic quantity, we use it here in a kinetic context because of its crucial role in determining the overall phase-transition rate. Hence, in this paper, we refer to the set of conditions for which the free-energy barrier is zero as a kinetic spinodal or stability limit. It has been shown elsewhere that knowledge of the locus of state points at which W_b vanishes is important in the correlation of nucleation rate data.[12−14]

Although the vanishing of the free-energy barrier provides an unambiguous condition for a kinetic limit of stability, the direct location of this condition is inevitably obscured by the fact that when the barrier height is of the order $k_B T$ (high superheating and supersaturation) thermal fluctuations alone provide enough activation energy for the system to climb the barrier. Consequently, under these conditions, it is highly improbable that the system can be found in the metastable minimum, and thus the properties of the metastable fluid itself are extremely difficult to determine. This kinetic manifestation represents a practically attainable limit of stability. Although there exists a wealth of data on practically attainable limits of stability,[2,15−22] their relation or proximity to corresponding absolute limits remains unknown. Thus, a definitive range of conditions over which a fluid can be metastable is uncertain, and one is often forced to rely on extrapolations of equations of state to obtain such information.

If, however, a highly metastable system could be prevented from relaxing toward stable equilibrium, then its properties could conceivably be determined. Although difficult to implement in a mathematical context, the rigorous imposition of constraints is comparatively easier in molecular simulation.[23−27] Crucial to these methods are the choice and severity of constraint used to maintain a sufficient degree of spatial homogeneity within the system, yet despite the mathematical rigor provided by constraint simulation approaches, such as restricted-ensemble Monte Carlo pioneered by Corti and co-workers,[24−27] their potential utility in the study of metastability remains unexplored.

Although direct (brute force) simulation methods are capable of determining the properties of metastable fluids, their range of application is limited to the vicinity of phase coexistence. In this region, the free-energy barrier is so high that it is extremely improbable that a metastable system is able to traverse it successfully, and thus the system remains in its local free-energy minimum. However, for moderately to highly metastable fluids, that is, conditions of practical interest, brute force simulations are inadequate. The reason for this is that the barrier height is sufficiently low under these conditions such that the system can traverse it with some probability of success. Thus, the natural tendency of a metastable system to relax toward equilibrium complicates the direct determination of its thermophysical properties. In the same spirit of constrained simulations, biased simulation methods, in particular, umbrella sampling,[28,29] have been developed to prevent the system from climbing the barrier too quickly within the finite duration of a simulation so that adequate statistics can be collected. This allows for adequate sampling of relatively high energy configurations that make an important contribution to the partition function of metastable systems. Recent advances in Monte Carlo simulation techniques, such as random-walk[30,31] and transition-matrix[32,33] algorithms, have provided highly efficient tools for exploring global phase behavior. The power of these techniques lies in their ability to sample high-energy points sufficiently in configuration space that would otherwise not be encountered in direct, brute force approaches. In principle, these more sophisticated sampling algorithms can be adapted to investigate metastable fluids and their stability limits. This is precisely what has been done in this work using transition-matrix Monte Carlo.

In this paper, we present results from a computational and theoretical study of liquid and vapor stability limits in the Lennard-Jones fluid. In particular, we use transition-matrix Monte Carlo[32,33] to calculate the particle number probability distribution. The simulation method and subsequent manipulation of the data represent a highly efficient methodology for predicting thermophysical properties of fluids over a wide range of conditions at a specified temperature. From the particle number distribution, we locate both kinetic and thermodynamic stability limits. As noted above, the former is defined mathematically to correspond to the condition at which the free-energy barrier separating the metastable state from the equilibrium fluid is zero, and the latter is where the fluid's thermodynamic response functions diverge. Although the intuitive expectation is that the kinetic and thermodynamic spinodals should coincide, we actually show from theoretical arguments that this must be the case for the liquid−vapor transition. A second, important finding in this work is the system-size dependence of the liquid and vapor spinodals. Although this system-size dependence has been noted by others in the simulation of lattice systems and supersaturated vapors,[34−41] we also present results for the superheated liquid.

The outline of this paper is as follows. In section II, we provide a brief overview of the transition-matrix Monte Carlo algorithm.[32,33] In addition, we present the theoretical formalism used in this work to locate both kinetic and thermodynamic spinodals. Given the theoretical nature of section II, we also show that kinetic and thermodynamic limits of stability for the liquid−vapor transition are equivalent. Computational details are discussed in section III. Results and discussion are presented in section IV. Finally, conclusions and directions for future work are given in section V.

II. Computational and Theoretical Methods

In this section, the computational and theoretical framework used in this study is presented. We first discuss the transition-matrix Monte Carlo algorithm[32,33] and its implementation in the grand canonical ensemble. Second, we show how to construct

an isotherm in the pressure−density plane from the particle number distribution calculated in the simulation, which in turn allows us to locate the thermodynamic limit of stability. Next, we show how to locate a kinetically defined limit of stability using straightforward histogram reweighting.[42] Finally, we show that the kinetically and thermodynamically defined spinodals are in fact one and the same in the case of the liquid−vapor phase transition.

A. Transition-Matrix Monte Carlo. Although transition-matrix Monte Carlo (TMMC) was originally introduced in the context of lattice systems,[32,33] only recently has its practical utility been demonstrated in the calculation of liquid−vapor surface tension and the determination of phase equilibria in continuum systems, in particular, the Lennard-Jones and square-well fluids.[43−46] The distinguishing feature of the algorithm is the accumulation of statistics regarding *attempted* transitions between states during the course of a Metropolis Monte Carlo simulation, as opposed to keeping track of states actually visited by the system. The result is a highly efficient sampling scheme that never discards data. In this subsection, we provide a brief overview of the algorithm followed by its implementation in the grand canonical ensemble. The details of the algorithm can be found elsewhere.[43,44]

In a traditional Metropolis Monte Carlo simulation,[47,48] a system is propagated along a Markov chain using a two-stage cycle. In the first stage of this cycle, a new microstate $t = t(\mathbf{r}_1,\mathbf{r}_2,...\mathbf{r}_N)$ is generated from the system's current microstate $s = s(\mathbf{r}_1,\mathbf{r}_2,...\mathbf{r}_N)$ with probability $q(s \rightarrow t)$. Although not strictly necessary, the selection matrix $q(s \rightarrow t)$ is usually designed to be symmetric in order to satisfy microscopic reversibility. In the second stage of the cycle, the new microstate t is conditionally accepted with probability $a(s \rightarrow t)$, which is given by the ratio of the proposed to the current microstate probabilities

$$a(s \rightarrow t) = \min\left[1, \frac{\pi(t)}{\pi(s)}\right] \tag{2}$$

where $\pi(t)$ and $\pi(s)$ represent the probabilities of observing the system in microstates t and s, respectively. To make a connection with the macroscopic properties of a system, it is assumed that each microstate s belongs to a macrostate S and accordingly microstate t belongs to macrostate T. For simplicity, S and T can be regarded as different values of some order parameter describing the system, such as the total energy, pressure, or bulk density. It follows that the probability of finding the system in macrostate S is a summation over all microstates that belong to it:

$$\Pi(S) = \sum_{s \in S} \pi(s) \tag{3}$$

The main objective here is to determine these macrostate probabilities because they are directly related to the system's equilibrium properties. A straightforward approach to doing this is simply to count the number of times the system visits a given state. In TMMC, the determination of the macrostate probabilities is performed in a more sophisticated and efficient manner. To this end, a third stage is added to the Metropolis algorithm where information regarding attempted transitions between macrostates is collected in a collection matrix **C**. Elements of the matrix are denoted by $C(S \rightarrow T)$ and contain statistics regarding attempted transitions from macrostate S to T. For any attempted or proposed Monte Carlo move taking the system from macrostate S to T, the collection matrix is updated according to the following rules:

$$C(S \rightarrow T) = C(S \rightarrow T) + a(s \rightarrow t) \tag{4}$$

and

$$C(S \rightarrow S) = C(S \rightarrow S) + 1 - a(s \rightarrow t) \tag{5}$$

It is important to emphasize that **C** is updated using eqs 4 and 5 for each proposed move regardless of whether it is accepted or rejected. To obtain an estimate of the macrostate probability distribution $\Pi(S)$ during a simulation, a macrostate transition probability matrix $P(S \rightarrow T)$ is first calculated from elements of the collection matrix **C**

$$P(S \rightarrow T) = \frac{C(S \rightarrow T)}{\sum_{\Delta S} C(S \rightarrow S + \Delta S)} \tag{6}$$

where $P(S \rightarrow T)$ represents the probability of the system moving from macrostate S to macrostate T provided that the system is currently in S. Employing a macroscopic detailed balance ansatz, namely, that

$$\Pi(S)\, P(S \rightarrow T) = \Pi(T)\, P(T \rightarrow S) \tag{7}$$

one can solve for $\Pi(S)$ in principle. This macroscopic detailed balance condition follows quite naturally in conventional Monte Carlo simulations where microscopic reversibility is maintained.[49] For nonconventional schemes, this is not necessarily the case. In eq 7, the macrostate transition probability $P(S \rightarrow T)$ represents elements from a stochastic matrix **P** whose stationary solution is Π with elements $\Pi(S)$. In general, this is an overspecified problem whose solution requires numerical minimization.[33] However, in this work, one can solve directly for Π because of our choice of macrostate variable and the types of trial moves performed in a grand canonical Monte Carlo (GCMC) simulation.

In the grand canonical ensemble (fixed volume V, temperature T, and chemical potential μ), the probability of observing a system in a microstate s is given by

$$\pi(s; \mu, V, T) = \frac{1}{\Xi(\mu, V, T)} \frac{V^{N(s)}}{\Lambda^{3N(s)} N(s)!} \exp[\beta\mu N(s)] \exp[-\beta E(s)] \tag{8}$$

where $N(s)$ is the number of particles in microstate s, Λ is the deBroglie wavelength, $E(s)$ is the potential energy of microstate s, β is the inverse temperature ($\beta = 1/k_B T$, k_B is the Boltzmann constant), and $\Xi(\mu, V, T)$ is the grand canonical partition function defined such that $\sum_s \pi(s; \mu, V, T) = 1$. A natural macrostate variable in the grand canonical ensemble is N, the number of particles in the system; this is equivalent to choosing the bulk density as a global order parameter. Thus, the objective is to determine the particle number distribution $\Pi(N; \mu, V, T)$, which is uniquely determined for a specified chemical potential μ, system volume V, and temperature T. Because only single-molecule insertion, deletion, and displacement moves are performed in a GCMC simulation, the macrostate transition probability matrix **P** is banded with three bands for this choice of macrostate variable. Employing detailed balance, eq 7, the relative macrostate probabilities can be evaluated sequentially:

$$\ln \Pi(N+1; \mu, V, T) = \ln \Pi(N; \mu, V, T) + \ln \frac{P(N \rightarrow N+1; \mu, V, T)}{P(N+1 \rightarrow N; \mu, V, T)} \tag{9}$$

Notice that to determine $\Pi(N; \mu, V, T)$ accurately in a GCMC simulation the system must be able to sample sufficiently both high and low particle numbers. Unfortunately, adequate sampling over such a broad range of particle numbers is usually unattainable because of the existence of an energy barrier separating liquidlike from vaporlike states, which is normally the case for sufficiently subcritical temperatures. To circumvent this bottleneck, a biasing potential $\eta(N)$ is introduced as is done in umbrella sampling[28,29] and so-called multicanonical sampling methods.[50] Ideally, $\eta(N)$ would be given by

$$\eta(N) = -\ln \Pi(N; \mu, V, T) \tag{10}$$

Because $\Pi(N; \mu, V, T)$ is not known a priori, in practice, $\eta(N)$ is updated regularly during a simulation with progressively more refined estimates of $\Pi(N; \mu, V, T)$, which provides a self-correcting approach to the true particle number distribution. One can show that the acceptance criteria for a trial move in the presence of a biasing function, $a_b(s \rightarrow t)$, is

$$a_b(s \rightarrow t) = \min\left\{1, \frac{\pi(t) \exp[\eta(T)]}{\pi(s) \exp[\eta(S)]}\right\} \tag{11}$$

Although the introduction of a biasing function modifies the acceptance criteria for trial moves, updating the collection matrix **C** remains the same as before in the absence of a bias, eqs 2, 4, and 5. It is precisely the simultaneous biasing of the simulation while using unbiased statistics to update the collection matrix that is responsible for the high efficiency of the TMMC algorithm.

B. Thermodynamic Approach to Spinodals. In this subsection, we show how to construct an isotherm in the pressure−density plane from the particle number distribution $\ln \Pi(N; \mu, V, T)$ calculated in a grand canonical TMMC simulation. We point out that the combination of the transition-matrix algorithm and manipulation of data outlined here provides an efficient tool for determining the thermophysical properties of fluids over a wide range of conditions. More importantly, notice that the construction of an equation of state allows for the application of well-defined thermodynamic stability criteria[11] to locate absolute liquid and vapor stability limits. The approach presented here provides an intuitive and transparent route to this objective.

Recall that $\Pi(N; \mu, V, T)$ is defined to be the probability of observing a system containing N particles at fixed chemical potential μ, volume V, and temperature T. From statistical mechanics,[51,52] this probability distribution can be expressed as

$$\Pi(N; \mu, V, T) = \frac{\exp(\beta\mu N)\, Q(N, V, T)}{\Xi(\mu, V, T)} \tag{12}$$

where $Q(N, V, T)$ is the canonical partition function. By writing $\Pi(N; \mu, V, T)$, we emphasize the fact that the particle number distribution is unique for given μ, V, and T. Taking the natural logarithm of both sides of eq 12 and rearranging terms, one obtains

$$\ln Q(N, V, T) = \ln \Pi(N; \mu, V, T) + \ln \Xi(\mu, V, T) - \beta\mu N \tag{13}$$

Recalling the statistical mechanical relation[51]

$$\beta A = -\ln Q(N, V, T) \tag{14}$$

where A is the Helmholtz free energy, eq 13 can be rewritten as

$$\beta A(N, V, T) = -\ln \Pi(N; \mu, V, T) - \ln \Xi(\mu, V, T) + \beta\mu N \tag{15}$$

Notice that $\Pi(N; \mu, V, T)$ is obtained from simulation. Furthermore, if the zero-particle limit is sampled, then the grand canonical partition function, or the grand potential $\beta\Omega = -\ln \Xi(\mu, V, T)$, is known exactly:[44,53,54]

$$-\beta\Omega(\mu, V, T) = \ln[\sum_N \Pi(N; \mu, V, T)] - \ln \Pi(0; \mu, V, T) \tag{16}$$

It is important to realize that eq 15 provides an expression for the Helmholtz free energy as a function of particle number at fixed temperature and volume. At this point, one could apply classical stability criteria, namely, that the curvature of the Helmholtz free energy with respect to particle number be positive.[11] However, to provide a physically intuitive discussion, we first determine the fluid's equation of state before proceeding to do so. Notice that the partial derivative of the free energy with respect to particle number under these constraints is a chemical potential

$$\mu(N, V, T) = \left(\frac{\partial A}{\partial N}\right)_{T,V} \tag{17}$$

where the dependence of the chemical potential on N, V, and T has been explicitly included to emphasize that this is the chemical potential in the canonical ensemble. An important subtlety to point out is that $\mu(N, V, T)$ is not necessarily the same quantity as the imposed chemical potential μ in the grand canonical ensemble.[39] To calculate an isotherm in the pressure−density projection of the phase diagram, we take a Legendre transform[11] of the Helmholtz free energy with respect to particle number, yielding an expression for the grand potential or $-pV$:

$$-pV = A(N, V, T) - \mu(N, V, T)N \tag{18}$$

Notice that each term on the right-hand side of eq 18 is a function of particle number. Because the volume of the system is fixed, one can therefore calculate pressure as a function of density at fixed temperature from $\Pi(N; \mu, V, T)$.

From classical thermodynamics, we know that for a pure substance at its limit of stability[11]

$$\left(\frac{\partial p}{\partial \rho}\right)_T = 0 \tag{19}$$

Therefore, the spinodal properties are simply given by their values at the relative extrema in the equation of state. Although other stability criteria exist, they are all violated simultaneously.[1,11] Our choice of eq 19 is based on convenience. Thus, the liquid and vapor spinodals can be determined straightforwardly by constructing an isotherm in the pressure−density plane and locating the relative extrema. We refer to the determination of the spinodal following this equation-of-state approach as a thermodynamic one. In section IV, we show that the spinodal properties of the Lennard-Jones liquid and vapor calculated by this thermodynamic approach possess a nonnegligible system-size dependence.

C. Kinetic Approach to Spinodals. In the previous subsection, we provided a thermodynamic route to locate limits of stability using the particle number distribution $\Pi(N; \mu, V, T)$ obtained from a grand canonical TMMC simulation. Here, we provide an alternative approach based on a kinetic viewpoint that relies on the calculation of free-energy barriers separating

the metastable state from the stable one. In this context, it is the vanishing of the energy barrier that signals the loss of stability, at which point the relaxation toward stable equilibrium is no longer an activated process but occurs spontaneously via spinodal decomposition.

The free energy W of a system as a function of some order parameter Φ is related to the probability distribution of that order parameter $\Pi(\Phi)$

$$\beta W(\Phi) = -\ln \Pi(\Phi) \tag{20}$$

where $\beta = 1/k_B T$. Recall that $\Pi(N; \mu, V, T)$ can be calculated from a TMMC simulation in the grand canonical ensemble (fixed chemical potential, volume, and temperature). Under these constraints, W corresponds to a grand potential free energy. Casting the problem in the language of kinetics, the particle number N, or bulk density ρ because the volume is fixed, therefore represents a global order parameter (reaction coordinate) describing the system as it changes from liquidlike to vaporlike densities or vice versa. Thus, eq 20 can be rewritten as

$$\beta W(N; \mu, V, T) = -\ln \Pi(N; \mu, V, T) \tag{21}$$

For conditions of interest, $W(N; \mu, V, T)$ has a double-well shape; that is to say, the particle number distribution is bimodal, where the higher-energy basin corresponds to the metastable state and the lower-energy basin corresponds to the stable equilibrium state. Separating these two is an energy barrier $W_b(\mu, V, T)$ whose height is simply

$$\beta W_b(\mu, V, T) = -\ln \frac{\Pi(N_{max}; \mu, V, T)}{\Pi(N_{min}; \mu, V, T)} \tag{22}$$

where N_{min} is the particle number corresponding to the location of the local relative minimum in the metastable basin and N_{max} is the particle number corresponding to the location of the local relative free-energy maximum. It should be emphasized that W_b is the energy barrier that the metastable system must traverse to transform into the stable state. Conceivably, one could insert the above barrier height into eq 1 and calculate a nucleation rate. Note that $N_{min} < N_{max}$ for a pure supersaturated vapor and $N_{min} > N_{max}$ for a pure superheated liquid. Let us now denote N_{spin}^{liq} as the largest particle number physically attainable by the liquid phase such that it remains homogeneous; accordingly, N_{spin}^{vap} is the highest particle number attainable by the vapor. Particle numbers intermediate between these limiting values correspond to an inhomogeneous system, that is, a mixture of liquid and gas. In other words, N_{spin}^{liq} and N_{spin}^{vap} are spinodal points, which we will explain how to locate below. With these definitions, the density of the liquid and vapor at specified μ, V, and T can be easily determined from the particle number distributions

$$\rho^{liq} = \frac{1}{V} \frac{\sum_{N_{spin}^{liq}}^{\infty} N\, \Pi(N; \mu, V, T)}{\sum_{N_{spin}^{liq}}^{\infty} \Pi(N; \mu, V, T)} \tag{23}$$

and

$$\rho^{vap} = \frac{1}{V} \frac{\sum_{0}^{N_{spin}^{vap}} N\, \Pi(N; \mu, V, T)}{\sum_{0}^{N_{spin}^{vap}} \Pi(N; \mu, V, T)} \tag{24}$$

Accordingly, the pressure of the liquid and vapor is given by

$$p^{liq} = \frac{1}{\beta V} \ln \frac{\sum_{N_{spin}^{liq}}^{\infty} \Pi(N; \mu, V, T)}{\Pi(0; \mu, V, T)} \tag{25}$$

and

$$p^{vap} = \frac{1}{\beta V} \ln \frac{\sum_{0}^{N_{spin}^{vap}} \Pi(N; \mu, V, T)}{\Pi(0; \mu, V, T)} \tag{26}$$

In practice, the upper limits of the summations in eqs 23 and 25 are replaced by the largest particle number sampled in the distribution.

Qualitatively, as the system becomes increasingly metastable, for instance, by varying the imposed chemical potential μ on the system, the thermodynamic driving force for the phase transformation, that is to say, the free-energy difference between the metastable and stable states, increases. Accordingly, the barrier height decreases and eventually vanishes. Mathematically, the free-energy profile $W(N; \mu, V, T)$ for which the energy barrier is zero is characterized by having an inflection point with zero slope. This condition constitutes what we define to be a kinetic spinodal.

To locate the kinetic spinodal using $\Pi(N; \mu, V, T)$, we employ histogram reweighting.[42] In particular, we determine the chemical potential value for which the free-energy profile contains an inflection point with zero slope. For illustrative purposes, let $\Pi(N; \mu_0, V, T)$ represent the particle number distribution calculated for a given system of volume V at temperature T and imposed chemical potential μ_0. From $\Pi(N; \mu_0, V, T)$, one can easily determine the corresponding distribution $\Pi(N; \mu, V, T)$ at some other chemical potential μ, where $\mu \neq \mu_o$, so long as the volume and temperature remain fixed. The relationship between $\Pi(N; \mu_0, V, T)$ and $\Pi(N; \mu, V, T)$ can be seen more clearly by recalling the statistical mechanical definition of the particle number probability distribution

$$\Pi(N; \mu_0, V, T) = \frac{\exp(\beta \mu_0 N)\, Q(N, V, T)}{\Xi(\mu_0, V, T)} \tag{27}$$

Solving for the canonical partition function $Q(N, V, T)$, substituting into eq 12, and then rearranging, one obtains

$$\ln \Pi(N; \mu, V, T) = \ln \Pi(N; \mu_0, V, T) + [\beta(\mu - \mu_0)N] + \ln \frac{\Xi(\mu_0, V, T)}{\Xi(\mu, V, T)} \tag{28}$$

In practice, because only free-energy differences are important, the last term in eq 28 can be neglected because it is just an additive constant. Therefore, a working expression for reweighting the probability distribution with respect to chemical potential is simply

$$\ln \Pi(N; \mu, V, T) = \ln \Pi(N; \mu_0, V, T) + [\beta(\mu - \mu_0)N] \quad (29)$$

Again, the overall strategy for locating the kinetic spinodal is simply to find the chemical potential for which the free-energy profile, or equivalently, $\ln \Pi(N; \mu, V, T)$, contains an inflection point with zero slope. For subcritical temperatures, there will be two chemical potential values for which this occurs: μ_{spin}^{liq} and μ_{spin}^{vap}, one for the liquid spinodal and the other for the vapor spinodal, respectively. If the saturation chemical potential is μ_{sat}, then $\mu_{spin}^{liq} < \mu_{sat} < \mu_{spin}^{vap}$. Accordingly, let N_{spin}^{liq} and N_{spin}^{vap} represent the locations of these particular inflection points in $\ln \Pi(N; \mu_{spin}^{liq}, V, T)$ and $\ln \Pi(N; \mu_{spin}^{vap}, V, T)$, respectively. Once the inflection points are located, fluid properties at the liquid spinodal can be calculated using $\ln \Pi(N; \mu_{spin}^{liq}, V, T)$, and those at the vapor spinodal, using $\ln \Pi(N; \mu_{spin}^{vap}, V, T)$. The density and pressure of the liquid at its limit of stability are

$$\rho_{spin}^{liq} = \frac{1}{V} \frac{\sum_{N=N_{spin}^{liq}}^{\infty} N \Pi(N; \mu_{spin}^{liq}, V, T)}{\sum_{N=N_{spin}^{liq}}^{\infty} \Pi(N; \mu_{spin}^{liq}, V, T)} \quad (30)$$

and

$$p_{spin}^{liq} = \frac{1}{\beta V} \ln \frac{\sum_{N=N_{spin}^{liq}}^{\infty} \Pi(N; \mu_{spin}^{liq}, V, T)}{\Pi(0; \mu_{spin}^{liq}, V, T)} \quad (31)$$

For practical purposes, the upper limits of the summations in eqs 30 and 31 are replaced by the largest particle number sampled in the distribution. By analogy, the density and pressure of the vapor at its stability limit are

$$\rho_{spin}^{vap} = \frac{1}{V} \frac{\sum_{N=0}^{N_{spin}^{vap}} N \Pi(N; \mu_{spin}^{vap}, V, T)}{\sum_{N=0}^{N_{spin}^{vap}} \Pi(N; \mu_{spin}^{vap}, V, T)} \quad (32)$$

and

$$p_{spin}^{vap} = \frac{1}{\beta V} \ln \frac{\sum_{N=0}^{N_{spin}^{vap}} \Pi(N; \mu_{spin}^{vap}, V, T)}{\Pi(0; \mu_{spin}^{vap}, V, T)} \quad (33)$$

D. Equivalence of the Kinetic and Thermodynamic Stability Limits. A priori, it is not at all obvious how a vanishing free-energy barrier (kinetic spinodal) is related to a diverging thermodynamic response function (thermodynamic spinodal). Although our intuitive expectation is that the two should coincide, it is unclear how to show that this must be true using rigorous statistical mechanics. Nevertheless, although the coincidence of these two conditions is merely an expectation, it is widely used to verify the validity of nucleation theories, and is supported by relatively recent simulations of nucleation phenomena.[55,56] Theoretically, the coincidence of a vanishing energy barrier with a thermodynamic limit of stability has been demonstrated only in theories that attempt to take into account local fluid structure, such as Cahn−Hilliard[57−59] and density-functional theory.[60] In this subsection, we show that the kinetic and thermodynamic spinodals are completely equivalent in the case of the liquid−vapor transition.

The starting point is eq 15, which provides an expression for the Helmholtz free energy as a function of particle number at fixed volume and temperature. One can directly apply thermodynamic stability criteria[11] to determine the thermodynamic spinodal condition, namely, that

$$\frac{\partial^2}{\partial N^2}[A(N, V, T)]_{T,V} = 0 \quad (34)$$

where the differentiation is performed at constant T and V. Differentiating eq 15 with respect to N twice, one can now express the stability limit condition in terms of the probability distribution $\Pi(N; \mu, V, T)$ as

$$\frac{\partial^2}{\partial N^2}[\ln \Pi(N; \mu, V, T)]_{T,V} = 0 \quad (35)$$

which states that the thermodynamic spinodal corresponds to an inflection point in the natural logarithm of the probability distribution calculated in grand canonical TMMC.

We now turn our attention to the kinetic spinodal. Recall that to locate the kinetic limit of stability we search for the chemical potential value, μ_{spin}^{vap} or μ_{spin}^{liq}, that gives rise to a free-energy profile that possesses an inflection point with zero slope. For simplicity, let μ_{spin} represent the spinodal chemical potential. Given $\Pi(N; \mu, V, T)$ calculated in a grand canonical TMMC simulation at chemical potential μ, volume V, and temperature T, the corresponding distribution $\Pi(N; \mu_{spin}, V, T)$ at chemical potential μ_{spin} and the same volume and temperature can be determined using histogram reweighting as before:

$$\ln \Pi(N; \mu_{spin}, V, T) = \ln \Pi(N; \mu, V, T) + [\beta(\mu_{spin} - \mu)N] + \ln \frac{\Xi(\mu, V, T)}{\Xi(\mu_{spin}, V, T)} \quad (36)$$

Differentiating both sides with respect to N twice at constant V and T yields the following important result

$$\frac{\partial^2}{\partial N^2}[\ln \Pi(N; \mu_{spin}, V, T)]_{T,V} = \frac{\partial^2}{\partial N^2}[\ln \Pi(N; \mu, V, T)]_{T,V} \quad (37)$$

which states that the curvature of the natural logarithm of the particle number distribution, or the free energy, is independent of the chemical potential at fixed volume and temperature. More importantly, in the present context, this implies that points of inflection in $\ln \Pi(N; \mu, V, T)$ are stationary with respect to μ. Therefore, because both the kinetic and thermodynamic limits of stability rely on locating these fixed points, they provide equivalent conceptual interpretations of the limit of stability.

However, although the kinetic and thermodynamic viewpoints are conceptually equivalent, the fluid properties at the spinodal so calculated differ slightly for finite-size systems. To understand why this is the case, consider how one determines the fluid density at a stability limit. Thermodynamically, the spinodal density is just N_{spin}/V. Kinetically, however, N_{spin} provides either an upper or lower limit over which to calculate an average particle number $\langle N \rangle$ (eqs 30 and 32). This average particle number divided by the system volume is the spinodal density as determined via the kinetic route. It should be obvious that $\langle N \rangle \neq N_{spin}$. In fact, one can easily show that the thermodynamically predicted vapor spinodal density is less than the kinetically predicted value and that the opposite is true in the case of the

liquid spinodal. We emphasize that the discrepancy noted here holds only for finite-size systems. In fact, we find that the differences decrease with increasing system size.

Although the arguments presented here are based on the grand canonical ensemble, the same conclusions can be reached by working in the isothermal−isobaric ensemble (fixed N, p, and T). In this case, the distribution of interest is the volume probability distribution, $\Pi(V; N, p, T)$, which can be expressed as

$$\Pi(V; N, p, T) = \frac{\exp(-\beta pV)\, Q(N, V, T)}{\Delta(N, P, T)} \tag{38}$$

where $\Delta(N, p, T)$ is the isothermal−isobaric partition function. The analogous working histogram reweighting expression with respect to pressure is

$$\ln \Pi(V; N, p, T) = \ln \Pi(V; N, p_0, T) + \beta(p_0 - p)V \tag{39}$$

where p_0 is the external pressure imposed in an actual isothermal−isobaric simulation. Using eqs 38 and 39, one can easily show that the thermodynamic and kinetic spinodals for the liquid−vapor transition are also equivalent in the isothermal−isobaric ensemble.

III. Simulation Details

In this section, we discuss the details of the simulations used to study liquid and vapor stability limits in the Lennard-Jones fluid. Particles in the system interact by a pairwise-additive potential of the form

$$u(r) = 4\epsilon\left[\left(\frac{\sigma}{r}\right)^{12} - \left(\frac{\sigma}{r}\right)^{6}\right] \tag{40}$$

where r is the interparticle distance, ϵ is the characteristic interaction energy, and σ is the characteristic length scale. In this work, we use the cut-and-shifted variant of this potential.[47] That is, the original interaction potential is truncated and shifted so that it goes to zero at a cutoff distance r_{cut}. Here, we let $r_{cut} = 4\sigma$.[56] Grand canonical TMMC simulations were performed at seven temperatures ($k_BT/\epsilon = 0.70$, 0.75, 0.80, 0.85, 0.90, 1.00, and 1.10), where the imposed chemical potential was chosen to be close to its saturation value. At each temperature, particle number probability distributions were calculated for three system volumes $V = L_{box}^3$ ($L_{box}/\sigma = 8$, 12, and 16). Grand canonical Monte Carlo moves consisted of 20% particle displacement and 80% insertion−deletion trials.

For simulations using a cubic simulation box of side length $L_{box}/\sigma = 8$ and 12, a single simulation run sufficed to generate particle number distributions that spanned the entire range of liquidlike and vaporlike values. These simulations were initiated with an empty simulation box and run for a minimum of 3×10^9 MC steps with the weighting function, eq 10, updated every 1×10^6 steps. For simulations using a box of side length $L_{box}/\sigma = 16$, a windowing scheme was implemented where the entire range of particle numbers was divided into sampling windows of width ΔN. The particle number probability distribution within each of these windows was determined via grand canonical TMMC, the only caveat being that insertion or deletion trial moves taking the system outside the particle number window were rejected outright. The distributions within each window were simply linked together by demanding that the free energy be a continuous function of particle number. Notice, too, that this approach lends itself well to very coarse-grained parallel processing. In this work, windows of size $\Delta N = 200$ were used, and a minimum of 2×10^9 MC steps were performed within each window.

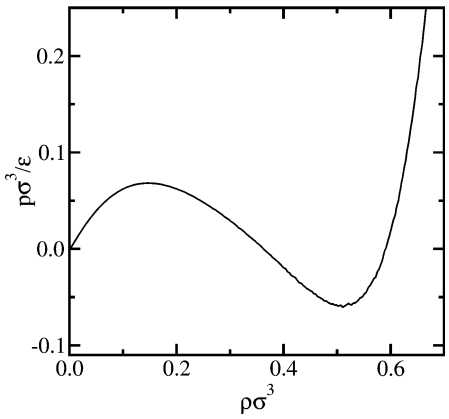

Figure 1. Isotherm ($k_BT/\epsilon = 1.10$) in the pressure−density plane for the Lennard-Jones fluid constructed from the particle number distribution calculated from grand canonical TMMC using a simulation box length $L_{box}/\sigma = 8$.

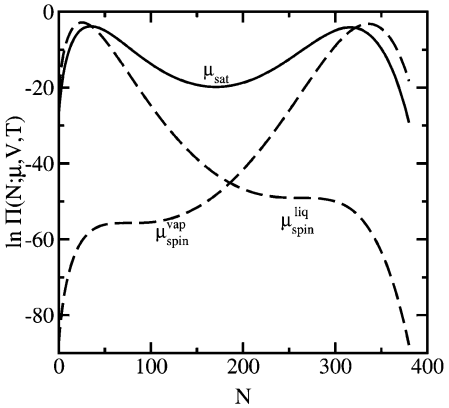

Figure 2. Particle number distributions at saturation μ_{sat}, the vapor spinodal μ_{spin}^{vap}, and liquid spinodal μ_{spin}^{liq} for $k_BT/\epsilon = 1.10$ and $L_{box}/\sigma = 8$. Note that $\mu_{spin}^{liq} < \mu_{sat} < \mu_{spin}^{vap}$.

IV. Results and Discussion

We have used grand canonical transition-matrix Monte Carlo simulation to investigate liquid and vapor stability limits in the Lennard-Jones fluid. To complement the discussion of section IIB, in Figure 1 we plot an isotherm ($k_BT/\epsilon = 1.10$) in the pressure−density plane constructed from a particle number distribution generated by a grand canonical TMMC simulation using a box length $L_{box}/\sigma = 8$. From this construction, the relative maximum and minimum yield the properties of the vapor and liquid spinodals, respectively (section IIB). From a conceptual standpoint, this equation-of-state route provides a transparent method to locating stability limits. Moreover, this is an efficient computational approach for determining thermophysical properties over a wide range of conditions.

In Figure 2, we plot the natural logarithm of the particle number probability distributions for the same temperature and simulation box size as in Figure 1 but at three different chemical potential values μ_{sat}, μ_{spin}^{vap}, and μ_{spin}^{liq}. The distributions were generated by histogram reweighting a particle number distribution calculated from grand canonical TMMC simulation using a chemical potential μ_0 whose value was chosen to be close to its saturation value. These curves provide the intuitive basis for the kinetic viewpoint of stability limits. The saturation chemical potential, μ_{sat}, was determined as the chemical potential for

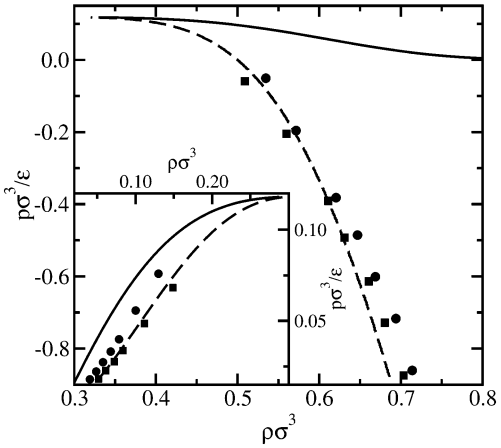

Figure 3. Thermodynamic (■) and kinetic (●) liquid spinodal points for the Lennard-Jones fluid at reduced temperatures (k_BT/ϵ) of 0.70, 0.75, 0.80, 0.85, 0.90, 1.00, and 1.10 using $L_{box}/\sigma = 8.0$. The inset shows the corresponding vapor spinodal points. The solid curve is the binodal predicted by the Johnson et al. equation of state.[61] The dashed curves are the spinodals predicted by the same equation of state.

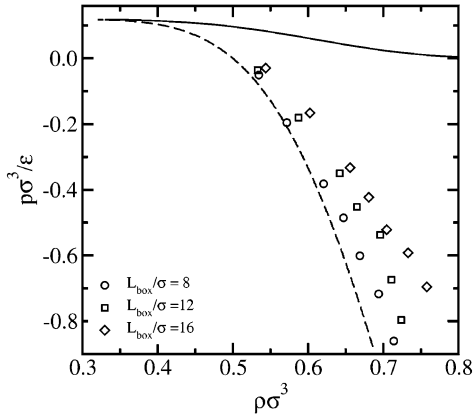

Figure 4. Kinetic stability limits for the Lennard-Jones liquid in the pressure−density plane as a function of system size at reduced temperatures (k_BT/ϵ) of 0.70, 0.75, 0.80, 0.85, 0.90, 1.00, and 1.10. The solid and dashed curves are the binodal and spinodal, respectively, predicted by the Johnson et al. equation of state.[61]

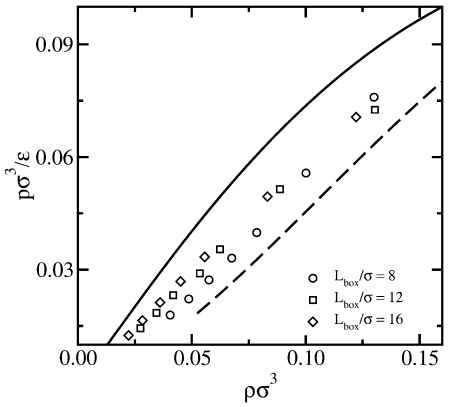

Figure 5. Kinetic stability limits for the Lennard-Jones vapor in the pressure−density plane as a function of system size at reduced temperatures (k_BT/ϵ) of 0.70, 0.75, 0.80, 0.85, 0.90, 1.00, and 1.10. The solid and dashed curves are the binodal and spinodal, respectively, predicted by the Johnson et al. equation of state.[61]

which the particle number distribution satisfied the so-called equal-area construction.[39,44] Because the free energy is just $-\ln \Pi(N; \mu, V, T)$, one can easily see that the free-energy barrier between the saturated liquid and vapor is finite for this particular simulation box size. As the chemical potential deviates further away from saturation, the free-energy difference between the metastable and stable states increases while the energy barrier that the metastable system must traverse decreases monotonically until it vanishes at the spinodal chemical potential. As can be seen in Figure 2, the vanishing of the barrier ultimately gives rise to a free-energy profile whose shape is fundamentally different from the familiar double-well form. In other words, stability loss is signaled when the particle number distribution changes from bimodal to unimodal. Once the spinodal chemical potential has been found and the inflection point has been located, eqs 30−33 can be used to calculate the fluid properties at their stability limit.

A comparison of the kinetically and thermodynamically defined liquid and vapor spinodals for the Lennard-Jones fluid is provided in Figure 3. The points given in Figure 3 were determined from grand canonical TMMC simulations using a box length $L_{box}/\sigma = 8$ for temperatures $k_BT/\epsilon = 0.70$, 0.75, 0.80, 0.85, 0.90, 1.00, and 1.10. For reference, we also show the binodal and spinodal curves calculated using the popular analytic Johnson et al. Lennard-Jones equation of state (EOS),[61] which is based on canonical molecular dynamics and Monte Carlo simulation data employing a particle number of 864 and a wide range of simulation box sizes. The original equation of state was modified to reflect the fact that the interaction potential was cut and shifted at 4σ. Details of this modification can be found in ref 61. In Figure 3, one can see that the thermodynamically predicted vapor spinodal agrees well with the Johnson et al. EOS, whereas the kinetically predicted vapor spinodal is shifted noticeably toward lower densities. In both cases, the deviation from the equation-of-state predictions increases with temperature. On the liquid side, the kinetic and thermodynamic spinodals agree relatively well with the Johnson et al. EOS, although the agreement in this case appears to improve with increasing temperature. Also, the kinetic stability limit of the liquid is shifted toward higher densities relative to the thermodynamic one. Finally, notice that the relative values of the kinetically and thermodynamically defined spinodal densities are entirely consistent with arguments presented at the end of section IID. Recall that the discrepancy is due to the fact that the fluid density at the thermodynamic stability limit is given by the location of the inflection point in $\ln \Pi(N, \mu, V, T)$ whereas the fluid density at the corresponding kinetic limit of stability involves averaging the particle number distribution over a range of particle numbers determined by N_{spin} (eqs 30 and 32). We find that the differences between the two approaches decrease with increasing system size.

Metastable fluids exist so long as they remain homogeneous. Because the probability of forming a critically sized nucleus (an inhomogeneity) somewhere within the system increases with system size, this implies that the region of metastability, and therefore, the spinodal, also depends on system size. In fact, practically attainable limits of stability measured in the laboratory are known to depend on sample size.[2,62,63] In Figures 4 and 5, we plot the kinetically defined liquid and vapor spinodals, respectively, for simulation box sizes $L_{box}/\sigma = 8$, 12, and 16 in the pressure−density projection of the phase diagram. For completeness, in Figures 6 and 7 the same data are plotted in the pressure−temperature plane. Again, for a point of reference, the binodal and spinodal curves calculated from the Johnson et al. EOS are also provided in the Figures. Notice in each case that the kinetic spinodal shifts toward the binodal as the simulation box size increases in accord with the preceding probabilistic arguments. Although agreement with the commonly

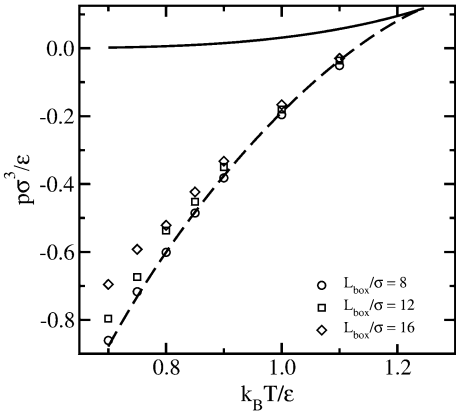

Figure 6. Kinetic stability limits for the Lennard-Jones liquid in the pressure−temperature plane as a function of system size. The solid and dashed curves are the binodal and liquid spinodal, respectively, as predicted by the Johnson et al. equation of state.

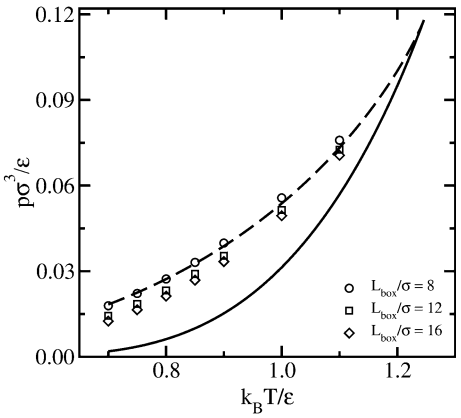

Figure 7. Kinetic stability limits for the Lennard-Jones vapor in the pressure−temperature plane as a function of system size The solid and dashed curves are the binodal and vapor spinodal, respectively, as predicted by the Johnson et al. equation of state.

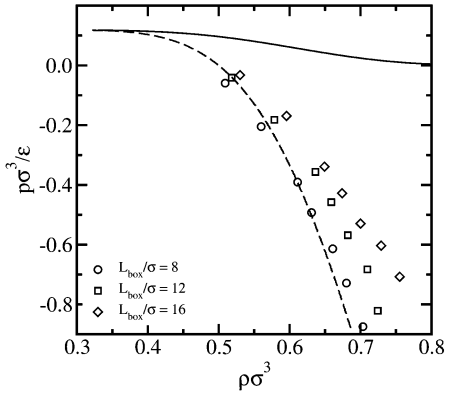

Figure 8. Thermodynamic stability limits for the Lennard-Jones liquid in the pressure−density plane as a function of system size. The solid and dashed curves are the binodal and liquid spinodal, respectively, as predicted by the Johnson et al. equation of state.

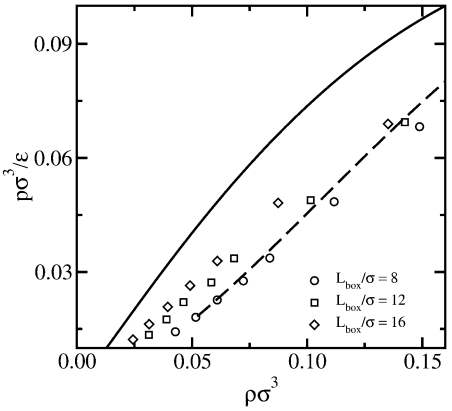

Figure 9. Thermodynamic stability limits for the Lennard-Jones vapor in the pressure−density plane as a function of system size. The solid and dashed curves are the binodal and vapor spinodal, respectively, as predicted by the Johnson et al. equation of state.

used Johnson et al. EOS is best for small simulation sizes, it is evident that the system-size dependence of the kinetically defined vapor and liquid spinodals is not at all negligible. In contrast, we point out that the saturation properties predicted by grand canonical TMMC are insensitive to the size of the system and agree with Gibbs ensemble results.[44]

In section IID, it was shown that the kinetically (vanishing free-energy barrier) and thermodynamically (diverging thermodynamic response functions) defined spinodals are conceptually equivalent viewpoints in that they both involved locating inflection points in the particle number probability distribution. Therefore, the thermodynamic spinodals determined via the construction outlined in section IIB should also depend on system size. In Figures 8 and 9, we plot the thermodynamic stability limits for the liquid and vapor, respectively. The trends in these two Figures are the same as those in the kinetic case, namely, that the spinodal moves toward the binodal with increasing system size. To rule out the possibility that the observed system-size effects were an artifact of performing simulations in an open ensemble, we performed TMMC simulations in the isothermal−isobaric ensemble.[44] As mentioned in section IID, the probability distribution of interest under these conditions is the volume probability distribution $\Pi(V; N, p, T)$, and accordingly, the spinodals correspond to inflection points in $\ln \Pi(V; N, p, T)$. In the isothermal−isobaric ensemble, we also find that the fluid properties at the spinodal approach their saturation values with increasing system size, which in this case is given by particle number N.

It should be noted that the results presented here do not represent the first evidence of system-size-dependent stability limits observed in computer simulation. System-size-dependent limits of stability were observed in early simulations of lattice systems[51] and have recently been revisited by Binder and others[34−41] to ascertain how the fluid properties at the spinodal should scale with the size of the system. Recently, MacDowell et al.[40] have used mean-field arguments to derive how the vapor spinodal should behave in the infinitely large system limit. Theoretically, they find that the vapor spinodal approaches the binodal in the infinitely large system limit, in particular, that

$$\left(\frac{\rho_{\text{spin}}^{\text{vap}}}{\rho_{\text{sat}}^{\text{vap}}} - 1\right) \sim \left(\frac{\xi}{V}\right)^{1/4} \tag{41}$$

where $\rho_{\text{spin}}^{\text{vap}}$ and $\rho_{\text{sat}}^{\text{vap}}$ are the vapor densities at the spinodal and saturation at the same temperature. ξ represents a characteristic length scale that MacDowell et al. have shown to be

$$\xi \propto \frac{(\beta\gamma)^3}{\rho_{\text{sat}}^{\text{vap}}\rho_{\text{sat}}^{\text{liq}\,2}} \tag{42}$$

where γ is the surface tension of a planar liquid−vapor interface. As noted by MacDowell et al., the physical implication of eq 41 is that the properties of the vapor at its stability limit approach

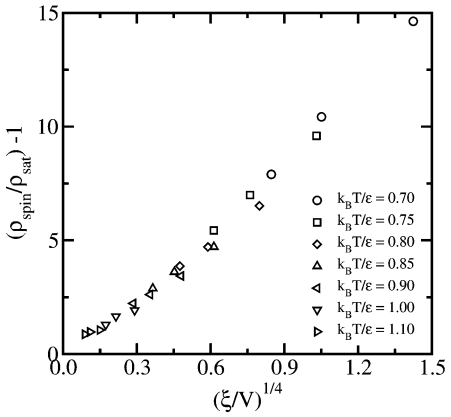

Figure 10. Scaling of the vapor density at the spinodal with system size using results generated by grand canonical TMMC simulation. The scaling variables were proposed by MacDowell et al. ξ is a characteristic length scale defined in the text.

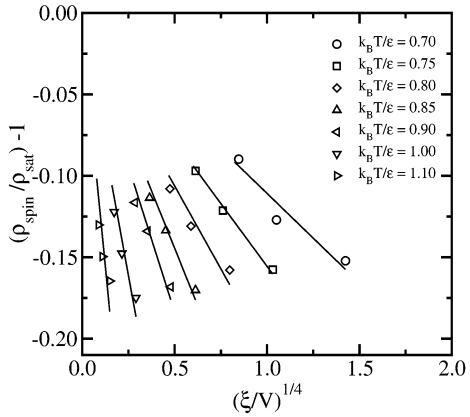

Figure 11. Scaling of the liquid density at the spinodal with system size using results generated by grand canonical TMMC simulation. The scaling variables were proposed by MacDowell et al. ξ is a characteristic length scale defined in the text.

their saturation values as the size of the system increases. In Figure 10, we test the proposed scaling of the vapor spinodal density with system size. The surface tension γ was determined by exploiting the finite-size scaling behavior of the free-energy barrier between the saturated liquid and vapor as discussed by Binder[64] and more recently by Errington.[43] The saturated densities were calculated using eqs 23 and 25 after finding the chemical potential for which the particle number distribution satisfied the equal-area construction.[44] As can be seen in Figure 10, the scaling proposed by MacDowell et al. works remarkably well for the vapor spinodal. It also appears that as the system size increases the spinodal vapor density converges to the saturated vapor density. Although the largest simulation box used in this study is moderately sized at best, computations involving much larger systems need to be performed to investigate the apparent convergence of the vapor spinodal with the binodal. It should be emphasized that the density scaling, eq 41, was derived specifically for the vapor. Although we are unaware of an analogous expression for the liquid, it is informative to test eq 41 against our results for the liquid spinodal, which is shown in Figure 11. Clearly, the density scaling does not hold for the liquid state, but it is apparent that the properties of the liquid at its limit of stability also approach their saturation values with increasing system size.

The results and discussion presented thus far appear to indicate that the liquid and vapor spinodals converge with the binodal in the infinitely large system limit; that is to say, the region of metastability for both the liquid and vapor vanishes. However, it should be emphasized that this is merely an extrapolation and, as such, should be interpreted with caution. Although our results are certainly consistent with this trend, they do not prove or disprove the notion of a vanishing region of metastability. Even if the fluid properties at the spinodal and binodal eventually coincide in the infinite system limit, the binodal and spinodal curves should still remain distinct from each other. To see why this is so, in Figure 12 we plot the density probability distribution at saturation at a reduced temperature $k_BT/\epsilon = 1.10$ as a function of system size. The density probability distribution is obtained from the particle number distribution by simply dividing the particle number by the volume of the system. One can see that the peaks and valleys in the distribution become more pronounced as the system size increases. At the same time, the inflection points in the distribution shift toward the locations of the peaks in the distribution, apparently suggesting an eventual convergence of the spinodal and binodal fluid properties. However, as discussed in section IID, a system at the brink of instability has a particle number, or density, distribution whose shape is fundamentally different from the bimodal distribution at saturation. More specifically, the distribution changes from bimodal to unimodal when the system becomes unstable. In other words, as the fluid becomes increasingly metastable, one of the peaks in the distribution must shrink and eventually vanish at the limit of stability. Under these conditions, the natural logarithm of the distribution possesses a second derivative with zero slope. This trend can be seen clearly in Figure 2. Although it is conceivable for the fluid properties at the spinodal and binodal to converge in the infinitely large system limit, the spinodal and binodal, however, remain distinct conditions because the corresponding particle number distributions must possess fundamentally different forms.

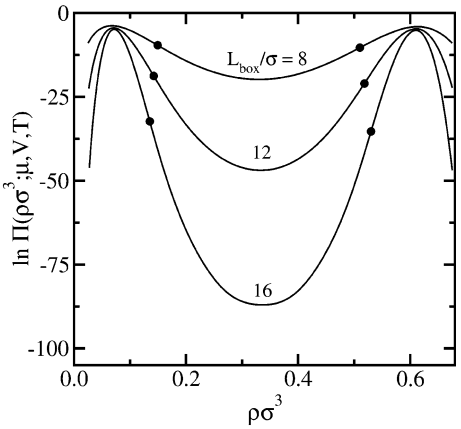

Figure 12. Size dependence of the density probability distribution at saturation at a reduced temperature $k_BT/\epsilon = 1.10$ using simulation box sizes $L_{box}/\sigma = 8$, 12, and 16. The inflections points are denoted by ●.

Interestingly, the existence of a spinodal curve has been the topic of intense debate for years. From a theoretical point of view, the consensus seems to be that the spinodal is simply a mean-field artifact.[1,65,66] Because mean-field theories do not incorporate local fluctuations, within the liquid−vapor coexistence dome for example, the phase-transformation mechanism changes sharply from nucleation, an *activated* process where the starting condition is metastable, to spinodal decomposition, a *spontaneous* process where the starting condition is inherently unstable. Therefore, in a mean-field theory, the transition from metastability to instability is very well defined and corresponds to the spinodal curve. However, in reality, this transition is not

sharply defined and actually occurs over a region due to local thermal fluctuations that can cause the system to traverse the free-energy barrier when the height is on the order k_BT. In fact, only in the thermodynamic limit and the limit of infinitely long-ranged and weak attractive interactions is the transition region from metastability to instability infinitely sharp as embodied in a spinodal curve.[27,67] Recent advances in experimental methods to monitor phase separation in polymeric systems, in particular, polymer blends, have demonstrated the importance of considering fluctuations in theories aimed at capturing the physics of these systems near their stability limit.[68−71] This is not to say that mean-field theories are completely inadequate in describing the phase behavior of metastable fluids or first-order phase transitions. The Ginzburg criterion[72] provides a quantitative means of determining when mean-field theory is adequate and when fluctuations are important. In simple fluids, the Ginzburg number is $\lambda^3(1 - T/T_{cr})$, where λ is the range of intermolecular interactions in units of characteristic molecular size and T_{cr} is the critical temperature. Only when the Ginzburg number is much greater than unity does mean-field theory apply. However, when the Ginzburg number is of order unity, this signals that localized fluctuations can no longer be neglected. At this point, thermal fluctuations alone are enough to trigger the transition from metastability to stable equilibrium. Clearly, the simulation results presented in this work account for fluctuations, but the density fluctuations in a grand canonical Monte Carlo simulation might not accurately reflect the type of localized fluctuations encountered in reality. In other words, bulk density might not be the appropriate order parameter or reaction coordinate in studying the liquid−vapor transition, which is a topic that has been discussed elsewhere.[14,55,73] Although only results for the cut-and-shifted Lennard-Jones fluid are presented in this work, we note in passing that analogous system-size trends are also observed in simulations incorporating the full Lennard-Jones potential.

From a practical perspective, we have provided convincing evidence that the stability limits of pure liquids and vapors are sensitive to the size of the system. Knowledge of the range over which a fluid is metastable is crucial to the study of nucleation phenomena. In computer simulation studies of nucleation in the Lennard-Jones liquid or vapor, the Johnson et al.[61] equation of state is commonly used to obtain an estimate of the metastability region of the fluid. However, we have shown that the Johnson et al. equation of state provides, at best, only a reasonable estimate of the liquid and vapor spinodal for small systems, which is to be expected because the EOS itself was based on simulations involving small system sizes. In fact, the EOS becomes inadequate for moderately sized systems, in particular, at sufficiently subcritical temperatures. Although using an analytic equation of state to locate spinodals is understandably far more convenient than performing a computer simulation, it should be emphasized that the simulation algorithm and subsequent manipulations outlined in section II represent a very fast and accurate approach for locating stability limits computationally.

V. Conclusions

In this paper, we have presented a highly efficient and straightforward methodology for locating pure liquid and vapor stability limits. The approach relies on the use of grand canonical transition-matrix Monte Carlo simulation to generate particle number probability distributions, that is to say, the probability of observing N particles in a system of volume V at temperature T and chemical potential μ. The particle number distribution can be subsequently manipulated to construct either a free-energy profile or an equation of state. The former construction provides a kinetically defined stability limit, which is located by determining the conditions for which the free-energy profile contains an inflection point with zero slope. In this work, this was done by reweighting the particle number distribution with respect to chemical potential. The latter construction, an equation of state, allows for the application of stability criteria to locate the so-called thermodynamic stability limit, which corresponds to the divergence of the fluid's thermodynamic response functions. We have shown that kinetic and thermodynamic spinodals are in fact conceptually equivalent with regard to the fact that both approaches rely on locating an inflection point in the free-energy profile or the natural logarithm of the particle number distribution.

Our results clearly demonstrate that liquid and vapor spinodals are system-size-dependent. For both the liquid and vapor, the fluid properties at the spinodal appear to approach their saturation values with increasing system size. This is in agreement with the simulation and theoretical work of others.[34−41] However, empirical observations of real macroscopic systems, which are presumably in the infinitely large system limit, indicate that metastable states do exist in reality. This suggests that the spinodal would in fact exhibit a limiting asymptotic behavior with increasing system size, where it would be distinct from the binodal. Moreover, in physical systems of macroscopic size, heat and mass transport phenomena become important issues, which have not been addressed here. Whether the spinodal converges with or is distinct from the binodal ultimately requires further investigation using larger systems than those used in this study.

Finally, having shown that limits of stability are dependent upon system size, one should exercise caution in using equations of state to provide estimates of the conditions over which a fluid is metastable, which is particularly important in studying nucleation phenomena using computer simulation. Furthermore, as is usually the case, the parameters of analytic equations of state are usually fit to stable data points, that is, conditions for which only one fluid phase is stable, and thus, using an EOS for stability-limit predictions can potentially take it outside its range of intended applicability. Instead, the methodology presented here provides a convenient alternative means to obtain highly accurate stability limit predictions via simulation.

Acknowledgment. V.K.S. gratefully acknowledges financial support from a National Research Council postdoctoral research associateship at the National Institute of Standards and Technology. J.R.E. acknowledges the financial support provided by startup funds from the University at Buffalo.

References and Notes

(1) Debenedetti, P. G. *Metastable Liquids: Concepts and Principles*; Princeton University Press: Princeton, NJ, 1996.
(2) *Nucleation*; Zettlemoyer, A. C., Ed.; Marcel Dekker: New York, 1969.
(3) Pockman, W. T.; Sperry, J. S.; O'Leary, J. W. *Nature* **1995**, *378*, 715−716.
(4) Holbrook, N. M.; Burns, M. J.; Field, C. B. *Science* **1995**, *279*, 1193−1194.
(5) Lush, P. A. *J. Fluid Mech.* **1983**, *135*, 373−387.
(6) Trevena, D. H. *Cavitation and Tension in Liquids*; Adam Hilger, Philadelphia, PA, 1987.
(7) Reid, R. C. *Am. Sci.* **1976**, *64*, 146−156.
(8) Reid, R. C. *Science* **1979**, *203*, 1265−1265.
(9) Evans, J. W.; DeJonghe, L. C. *The Production of Inorganic Materials;* Macmillan Publishing: New York, 1991.
(10) Mullin, J. W. *Crystallization*,3rd ed.; Butterworth: Oxford, England, 1993.

(11) Tester, J. W.; Modell, M. *Thermodynamics and Its Applications*, 3rd ed.; Prentice Hall: Upper Saddle River, NJ, 1997.
(12) McGraw, R.; Laaksonen, A. *Phys Rev. E* **1996**, *76*, 2754−2757.
(13) Talanquer, V. *J. Chem. Phys.* **1997**, *106*, 9957−9960.
(14) Shen, V. K.; Debenedetti, P. G. *J. Chem. Phys.* **2001**, *114*, 4149−4159.
(15) Blander, M.; Katz, J. L. *J. Stat. Phys.* **1972**, *4*, 55−59.
(16) Blander, M.; Katz, J. L. *Am. Inst. Chem. Eng. J.* **1975**, *21*, 833−848.
(17) Williamson, S.; Mourou, G.; Li, J. C. M. *Phys. Rev. Lett.* **1984**, *52*, 2364−2367.
(18) Avedisian, C. T. *J. Phys. Chem. Ref. Data* **1985**, *14*, 695−729.
(19) Hixson, R. S.; Boness, D. A.; Shaner, J. W.; Moriarty, J. A. *Phys. Rev. Lett.* **1989**, *62*, 637−640.
(20) Baidakov, V. G.; Skripov, V. P. *Exp. Therm. Fluid Sci.* **1992**, *5*, 664−678.
(21) Herman, J. W.; Elsayed-Ali, H. E. *Phys. Rev. Lett.* **1992**, *69*, 1228−1231.
(22) Murphy, E. A.; Elsayed-Ali, H. E.; Herman, J. W. *Phys. Rev. B* **1993**, *48*, 4921−4924.
(23) Carter, E. A.; Ciccotti, G.; Haynes, J. T.; Kapral, R. *Chem. Phys. Lett.* **1989**, *156*, 472−476.
(24) Corti, D. S.; Debenedetti, P. G. *Chem. Eng. Sci.* **1994**, *49*, 2717−2734.
(25) Corti, D. S.; Debenedetti, P. G. *Ind. Eng. Chem. Res.* **1995**, *34*, 3573−3580.
(26) Corti, D. S.; Debenedetti, P. G.; Sastry, S.; Stillinger, F. H. *Phys. Rev. E* **1997**, *55*, 5522−5534.
(27) Corti, D. S.; Debenedetti, P. G. *Phys. Rev. E* **1998**, *57*, 4211−4226.
(28) Torrie, G. M.; Valleau, J. P. *Chem. Phys. Lett.* **1974**, *28*, 578−581.
(29) Torrie, G. M.; Valleau, J. P. *J. Comput. Phys.* **1977**, *23*, 187−199.
(30) Wang, F.; Landau, D. P. *Phys. Rev. Lett.* **2001**, *86*, 2050−2053.
(31) Wang, F.; Landau, D. P. *Phys. Rev. E* **2001**, *64*, 056101.
(32) Fitzgerald, M.; Picard, R. R.; Silver, R. N. *Europhys. Lett.* **1999**, *46*, 282−287.
(33) Fitzgerald, M.; Picard, R. R.; Silver, R. N. *J. Stat. Phys.* **2000**, *98*, 321−345.
(34) Furukawa, H.; Binder, K. *Phys. Rev. A* **1982**, *26*, 556−566.
(35) Kaski, K.; Binder, K.; Gunton, J. D. *Phys. Rev. B: Condens. Matter* **1984**, *29*, 3996−4009.
(36) Kido, A.; Kitao, O.; Nakanishi, K. *Chem. Phys. Lett.* **1992**, *199*, 403−407.
(37) Imre, A.; Martinas, K.; Rebelo, L. P. N. *J. Non-Equilib. Thermodyn.* **1998**, *23*, 351−375.
(38) Binder, K. *Physica A* **2003**, *319*, 99−114.
(39) MacDowell, L. G. *J. Chem. Phys.* **2003**, *119*, 453−463.
(40) MacDowell, L. G.; Virnau, P.; Muller, M.; Binder, K. *J. Chem. Phys.* **2004**, *120*, 5293−5308.
(41) Neuhaus, T.; Hager, J. S. *J. Stat. Phys.* **2003**, *113*, 47−83.
(42) Ferrenberg, A. M.; Swendsen, R. H. *Phys. Rev. Lett.* **1988**, *61*, 2635−2638.
(43) Errington, J. R. *Phys. Rev. E* **2003**, *67*, 012102.
(44) Errington, J. R. *J. Chem. Phys.* **2003**, *118*, 9915−9925.
(45) Singh, J. K.; Kofke, D. A.; Errington, J. R. *J. Chem. Phys.* **2003**, *119*, 3405−3412.
(46) Shell, M. S.; Debenedetti, P. G.; Panagiotopoulos, A. Z. *J. Chem. Phys.* **2003**, *119*, 9406−9411.
(47) Allen, M. P.; Tildesley, D. J. *Computer Simulation of Liquids*; Oxford University Press: Oxford, England, 1996.
(48) Frenkel, D.; Smit, B. *Understanding Molecular Simulation*, 2nd ed.; Academic Press: San Diego, CA; 2002.
(49) Wang, J.-S.; Swendsen, R. H. *J. Stat. Phys.* **2002**, *106*, 245−285.
(50) Berg, B. A.; Neuhas, T. *Phys. Rev. Lett.* **1992**, *68*, 9−12.
(51) Hill, T. L. *Statistical Mechanics: Principles and Applications*; Dover: New York, 1987.
(52) Hill, T. L. *Thermodynamics of Small Systems;* Dover: New York, 1994.
(53) Errington, J. R.; Panagiotopoulos, A. Z. *J. Phys. Chem. B* **1999**, *103*, 6314−6322.
(54) Panagiotopoulos, A. Z. *J. Phys.: Condens. Matter* **2000**, *12*, 25−52.
(55) Shen, V. K.; Debenedetti, P. G. *J. Chem. Phys.* **1999**, *111*, 3581−3589.
(56) Punnathanam, S.; Corti, D. S. *Ind. Eng. Chem. Res.* **2002**, *41*, 1113−1121.
(57) Cahn, J. W.; Hilliard, J. E. *J. Chem. Phys.* **1958**, *42*, 93.
(58) Cahn, J. W. *J. Chem. Phys.* **1959**, *30*, 1121.
(59) Cahn, J. W.; Hilliard, J. E. *J. Chem. Phys.* **1959**, *31*, 688.
(60) Oxtoby, D. W.; Evans, R. *J. Chem. Phys.* **1988**, *89*, 7521−7530.
(61) Johnson, J. K.; Zollweg, J. A.; Gubbins, K. E. *Mol. Phys.* **1993**, *78*, 591−618.
(62) Eberhart, J. G.; Kremsner, W.; Blander, M. *J. Colloid Interface Sci.* **1975**, *50*, 369−378.
(63) Porteous, W.; Blander, M. *AIChE J.* **1975**, *21*, 560−566.
(64) Binder, K. *Phys. Rev. A* **1982**, *25*, 1699−1709.
(65) Unger, C.; Klein, W. *Phys. Rev. B* **1984**, *29*, 2698−2708.
(66) Novotony, M. A.; Klein, W.; Rikvold, P. *Phys Rev. B* **1986**, *33*, 7729−7737.
(67) Lebowitz, J. L.; Penrose, O. *J. Math. Phys.* **1966**, *7*, 98−113.
(68) Wood, S. M.; Wang, Z.-G. *J. Chem. Phys.* **2002**, *116*, 2289−2300.
(69) Wang, Z.-G. *J. Chem. Phys.* **2002**, *116*, 2289−2300.
(70) Lefebvre, A. A.; Lee, J. H.; Balsara, N. P.; Vaidyanathan, C. *J. Chem. Phys.* **2002**, *117*, 9063−9073.
(71) Lefebvre, A. A.; Lee, J. H.; Balsara, N. P.; Vaidyanathan, C. *J. Chem. Phys.* **2002**, *117*, 9074−9083.
(72) Binder, K. *Phys. Rev. A* **1984**, *29*, 341−349.
(73) Shen, V. K.; Debenedetti, P. G. *J. Chem. Phys.* **2003**, *118*, 768−783.